Chemical Science

ROYAL SOCIETY OF CHEMISTRY

EDGE ARTICLE

View Article Online
View Journal | View Issue

Cite this: *Chem. Sci.*, 2022, **13**, 5687

All publication charges for this article have been paid for by the Royal Society of Chemistry

Achieving highly selective CO_2 adsorption on SAPO-35 zeolites by template-modulating the framework silicon content†

Yan Li,‡[a] Hongwei Chen,‡[b] Chaoran Wang,[a] Yu Ye,[a] Libo Li,[b] Xiaowei Song *[a] and Jihong Yu *[ac]

Received 4th February 2022
Accepted 18th April 2022

DOI: 10.1039/d2sc00702a

rsc.li/chemical-science

Small-pore silicoaluminophosphate (SAPO) zeolites with 8-ring pore windows and appropriate acidities/polarities, for example, SAPO-34 (**CHA**) and SAPO-56 (**AFX**), have proven to be potential adsorbing materials for selective adsorption of CO_2. However, SAPO-35 zeolites (**LEV** framework topology) synthesized using conventional templates are less reported for highly selective CO_2 adsorption which might be due to inappropriate Si contents and acidities in the framework. In this work, by using *N*-methylpiperidine (NMP) as a template, SAPO-35 zeolites with various Si contents were synthesized under hydrothermal conditions, which allowed SAPO-35 zeolites with modulated acidities and polarities. The CO_2 adsorption and separation properties of SAPO-35_*x* (*x*: Si/(Si + P + Al) in molar ratio) were investigated, and a close relationship between the acidity, polarity and CO_2 adsorption and separation capacity was revealed. SAPO-35_0.14 with the strongest acidity showed the highest CO_2 uptake of 4.76 mmol g^{-1} (273 K and 100 kPa), and appeared to be one of the best SAPO materials for CO_2 adsorption. Moreover, increased Brønsted acidity can significantly enhance the adsorption selectivity of CO_2 over N_2. At 298 K and 100 kPa, SAPO-35_0.14 showed the highest CO_2/N_2 selectivity of 49.9, exhibiting potential for industrial processes. Transient binary breakthrough experiments on SAPO-35_0.14 further proved the efficient separation performance and stable circulation. The results of this study prove that the framework Si content of SAPO-35 zeolites is essential for regulating their CO_2 adsorption performance. This work demonstrates that modulating the silicon content and acidity in SAPO zeolites *via* a suitable choice of template, as well as polarity, is of great significance for the rational synthesis of zeolites with superior CO_2 adsorption and separation abilities.

Introduction

The release of greenhouse gases, especially CO_2 arising from fossil fuel combustion, has caused global warming and extreme weather, which upset the balance of the ecosystem. CO_2 capture and separation from effluent gases has thus attracted more and more attention. Flue gas emissions coming from power plants account for 33–40% of total CO_2 emissions, and N_2 is the major component of the flue gas (>70%).[1] Currently, the most widely adopted technology for the separation of CO_2/N_2 mixed gases, *i.e.*, aqueous amine absorption, causes a large quantity of energy consumption and waste. Thus, it is necessary to promote the development of physical adsorption technologies with lower energy penalty and lower cost, for example pressure swing adsorption (PSA).[1,2] Among physical adsorption technologies, the investigation and evolution of highly efficient adsorbing materials is the focus of adsorption and separation.[3] In recent years, porous solid adsorbing materials such as zeolites,[4] metal–organic frameworks (MOFs),[5] zeolitic imidazolate frameworks (ZIFs),[6] covalent organic frameworks (COFs),[7] and porous organic polymers (POPs)[8] have been extensively used in selective adsorption. Among these adsorbents, MOFs show potential because of their controllable structures and functions but are limited by the weak thermal stability and high manufacturing costs.[9]

Zeolites are a famous category of inorganic porous materials with well-defined and stable structures, large surface areas, and various active sites, which have broad applications in the fields of catalysis, ion exchange, adsorption/separation and pharmaceuticals.[10] The large CO_2 adsorption capacity, high structural

[a]*State Key Laboratory of Inorganic Synthesis and Preparative Chemistry, College of Chemistry, Jilin University, 2699 Qianjin Street, Changchun 130012, P. R. China. E-mail: xiaoweisong@jlu.edu.cn; jihong@jlu.edu.cn*

[b]*College of Chemical Engineering and Technology, Shanxi Key Laboratory of Gas Energy Efficient and Clean Utilization, Taiyuan University of Technology, Taiyuan 030024, P. R. China*

[c]*International Center of Future Science, Jilin University, 2699 Qianjin Street, Changchun 130012, P. R. China*

† Electronic supplementary information (ESI) available: Details of the synthesis, characterization and calculations of SAPO-35_*x*. See https://doi.org/10.1039/d2sc00702a

‡ These authors contributed equally.

stability and controllable polarity give zeolites great potential for application in gas adsorption and separation of CO_2-containing gas mixtures.[11] Zeolites preferentially adsorb molecules with large dipole and quadrupole moments, especially CO_2 (13.4×10^{-40} C m^2 quadrupole moment), because the frameworks possess strong electric fields, and thus fairly high CO_2 adsorption uptake and selectivity over N_2 (4.7×10^{-40} C m^2 quadrupole moment) at low pressure, making them promising candidates for applications.[4a,12] Various factors can influence the adsorption capacity and selectivity of zeolites for CO_2, such as framework composition,[13] topologies,[14] channel systems,[15] pore size dimensions,[16] pore volumes,[17] exchanged cations,[18] isomorphous heteroatom substitutions,[19] and numbers and distributions of active sites that are related to acidities and polarities.[12b,20] It is worth noting that the similar kinetic diameters of CO_2 (0.33 nm) and N_2 (0.36 nm) make kinetic separation very challenging.[9,21] Recently, some small pore zeolites with 8-membered ring windows have been spotlighted and confirmed to be excellent CO_2 adsorbents, since the effective size of their 8-rings can be tuned to ensure the passage of CO_2, but to hinder the slightly larger N_2 molecule, leading to high CO_2/N_2 selectivity.[4a,14,20,22] As a notable example, the low-pressure separation of CO_2 from N_2 by SSZ-13 zeolite (**CHA** framework topology) was studied in both acidic and copper-exchanged forms, which exhibited unconventional high selectivity (>70) evaluated by the ideal adsorbed solution theory under ideal conditions for industrial CO_2/N_2 separations.[4a] The high CO_2 uptake of aluminosilicate zeolites is partly due to their high electrical field gradients. However, aluminosilicate zeolites adsorb CO_2 very vigorously, limiting the ease of their use in cyclic adsorption processes.[12c,23]

Silicoaluminophosphate (SAPO) zeolites, which are an important category of zeolites, provide equally high CO_2 adsorption capacity as adsorbents at corresponding pressures. Their weaker electrical field gradients lead to highly reversible CO_2 uptake.[24] For instance, SAPO-56 displayed a higher CO_2 adsorption uptake (5.42 mmol g^{-1} at 273 K and 101 kPa) and less water sensitivity than aluminosilicate zeolite 13X. Cyclic adsorption and *in situ* infrared spectroscopy (IR) revealed that SAPO-56 retained 95% of its initial CO_2 capacity after six cycles and that adsorption occurred *via* physisorption.[24a]

SAPO-35 with **LEV** topology will be a preferred candidate for CO_2 adsorption and separation due to its structural features. Levyne (**LEV**) is a typical small pore 8-ring window zeolite belonging to the ABC-6 family constructed by ***lev*** cages, single 6-rings and double 6-rings, whose window dimensions (0.36 × 0.48 nm) allowing the molecules to diffuse through are very suitable for the separation of CO_2 from N_2.[24a,25] However, few studies have focused on the investigation of Levyne and its analogues for CO_2 adsorption and separation. The SAPO-35 zeolites were typically synthesized by using hexamethyleneimine (HMI) as a template which showed a poor CO_2 adsorption capacity.[24a] This might be due to the inappropriate Si acidities/polarities in the framework. Herein, by adopting *N*-methylpiperidine (NMP) as a template, a series of SAPO-35 zeolites were synthesized, which exhibited a wider range of Si content from 5% to 23%. The relationship between Si content and CO_2 adsorption and separation abilities was also investigated. By regulating the Si content in SAPO-35 zeolites synthesized using NMP, we found that the sample with moderate Si content showed the strongest Brønsted acidity and polarity, further aiding in CO_2 affinity and separation of the CO_2/N_2 mixture. This work implies that many small pore SAPO zeolites could be explored for gas adsorption and separation applications by template assisted modulation of the Si content to tune the framework acidity and polarity.

Results and discussion

Synthesis and characterization

Three SAPO-35_*x* samples with different Si contents were synthesized using NMP as a template under hydrothermal conditions at 180 °C. The molar composition of the starting mixture was 1.0 Al_2O_3 : 2.0 P_2O_5 : *n* SiO_2 : 6.15 NMP : 123.8 H_2O (n = 0.2, 0.6, or 1.4). The powder X-ray diffraction patterns are all consistent with that of a previously reported zeolite with the **LEV** topology,[25] proving their phase purity (Fig. S1†). The scanning electron microscopy (SEM) images of SAPO-35_*x* samples show cube-like rhombohedral morphology (Fig. S2†), and the variation of Si content leads to a change of product size from 15 μm to 40 μm. Inductively coupled plasma atomic emission spectrum (ICP-AES) analyses give SAPO-35_*x* samples with Si contents of 0.08, 0.14 and 0.22 in molar ratio (Table S1†). N_2 adsorption–desorption isotherms were measured at 77 K to characterize the porous properties of SAPO-35_*x* samples. As shown in Fig. 1, all the samples display characteristic type I isotherms according to the IUPAC classification, confirming their microporous characteristics. As shown in Table S1,† the Brunauer–Emmett–Teller (BET) specific surface areas are calculated to be 493 m^2 g^{-1} for SAPO-35_0.08, 502 m^2 g^{-1} for SAPO-35_0.14, and 447 m^2 g^{-1} for SAPO-35_0.22 in the pressure range 0.05–0.30 P/P_0. Micropore volumes of SAPO-35_0.08, SAPO-35_0.14, and SAPO-35_0.22 are 0.22, 0.22, and 0.18 cm^3 g^{-1} determined by the *t*-plot method, respectively. The above values are similar to those of previously reported SAPO-35

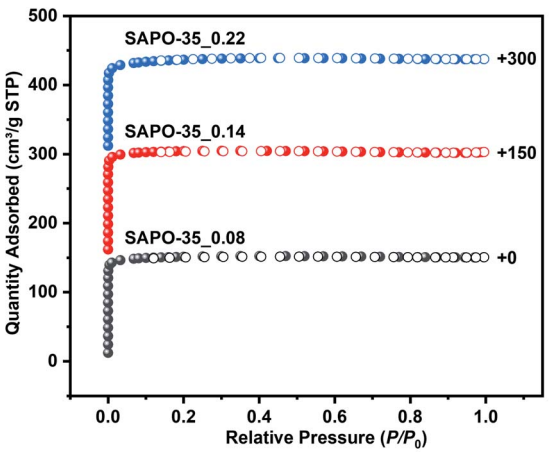

Fig. 1 N_2 adsorption–desorption isotherms of SAPO-35_*x* samples at 77 K.

zeolites in the literature.[26] The decrease of BET specific surface area and micropore volume of SAPO-35_0.22 is based on the decrease in crystallinity, which is also proved by the decrease in XRD peak intensity in Fig. S1.† Temperature-programmed desorption of ammonia (NH_3-TPD) was employed to determine the acidity of the SAPO-35_x samples (Fig. S3†). The desorption temperature indicates the acidic strength, and the peak area indicates the acidic concentration of the samples. Obviously, SAPO-35_0.14 with medium Si content possesses the strongest acid strength and the highest concentration of acid sites among these three samples.

Subsequently, solid-state ^{29}Si MAS NMR spectra were measured to clarify the relationship between Si content and acidity. The silicon substitution proceeds *via* the SM2 mechanism (for low Si content) and SM2 + SM3 mechanism. In case of the SM2 mechanism, only P atoms are substituted, causing Brønsted acidity, while for the SM3 mechanism, an (Al, P) pair is substituted by two Si atoms. When the degree of Si substitution in SAPO zeolites is high enough to generate Si islands, *i.e.*, Si(4Si,0Al), there is a decrease in the acidity of SAPO zeolites.[27] ^{29}Si MAS NMR spectra of SAPO-35_x samples are shown in Fig. S4.† The peaks at −90 and −95 ppm in SAPO-35_0.08 can be assigned to the Si(0Si,4Al) unit at the T1 and T2 sites in the SAPO-35 framework, respectively. With the increase of Si content (SAPO-35_0.14; SAPO-35_0.22), the coordination environments of Si become complex, and the peaks for Si(nSi,(4−n)Al) (n = 0 to 4) become overlapped between −90 ppm and −110 ppm. In general, peaks at around −110 ppm can be assigned to Si(4Si,0Al), which appears only in SAPO-35_0.22, leading to its decrease of acidity compared to SAPO-35_0.14.[25]

CO_2 adsorption

Pure CO_2 adsorption isotherms of SAPO-35_x samples were measured at 273, 283 and 298 K, respectively, to evaluate the CO_2 adsorption abilities of SAPO-35 zeolites with different Si contents and acidity. As shown in Fig. 2 and Table 1, the CO_2 uptakes of these SAPO-35 samples decrease with increase in temperature, and are always in the order SAPO-35_0.14 > SAPO-35_0.22 > SAPO-35_0.08 at 273, 283, and 298 K and 100 kPa whether in the low-pressure area or in the high-pressure area. The results clearly show that Si contents regulated by the template and the enhanced acidity could strengthen the CO_2 adsorption capacity of SAPO-35 zeolites. Compared with other pure AlPO zeolites and SAPO zeolites, SAPO-35_0.14 (4.76 mmol g^{-1} at 273 K and 100 kPa) appears to be one of the best AlPO/SAPO zeolite adsorbents for CO_2 adsorption (Table S2†), which is superior to aluminosilicate zeolites with the same topology (Na-LEV)[28] and most of the SAPO zeolites, proving the potential of SAPO-35 zeolites in CO_2 adsorption.

Obviously, the framework Si content of SAPO-35 zeolites plays an essential role in governing the CO_2 adsorption behaviour of this structure type of small-pore zeolites. To further explore the relationship between CO_2 adsorption properties, Si content and acidity in SAPO-35_x zeolites, the isosteric heats of CO_2 adsorption (Q_{st}) for SAPO-35_x zeolites were calculated by fitting the CO_2 adsorption isotherms at 273, 283 and 298 K to the virial equation (Fig. S5†). As shown in Table 1 and Fig. 2d, the Q_{st} at zero coverage for SAPO-35_0.14 (29.3 kJ mol^{-1}) is the highest among the three SAPO-35_x samples. The result indicates that increased acidity could strengthen the interaction between the CO_2 adsorbate and the inorganic framework. The regeneration of the adsorbent is one of the most important parameters for practical application. One way to estimate the regeneration of an adsorbent is the determination of the energy released during the adsorption process by means of Q_{st}. Excessive Q_{st} of aluminosilicate zeolites will be against the desorption of CO_2, thus leading to low regenerability and high-energy cost.[4a] SAPO-35 zeolites possess medium Q_{st} and relatively high CO_2 adsorption, which are beneficial to the application for CO_2 adsorption/desorption.

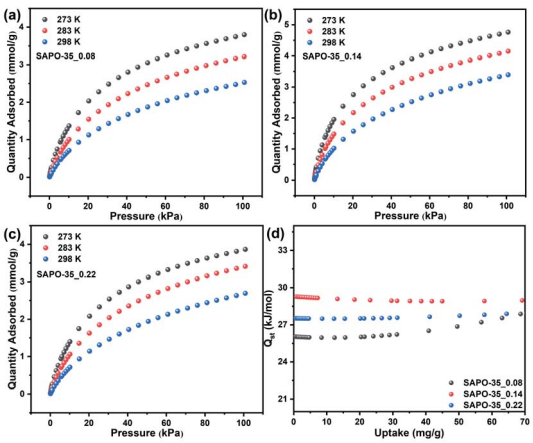

Fig. 2 CO_2 adsorption of (a) SAPO-35_0.08, (b) SAPO-35_0.14, and (c) SAPO-35_0.22 at 273, 283 and 298 K. (d) Isosteric heat of adsorption (Q_{st}) for the SAPO-35_x samples.

CO_2/N_2 selectivity predicted by ideal adsorbed solution theory (IAST)

Apparently, CO_2 is more favorably adsorbed than N_2 on all SAPO-35_x samples. The size and electronic properties of CO_2 and N_2 are shown in Table S3.† The kinetic diameter of CO_2 is smaller, and hence it can more easily diffuse into the **LEV** pore structure (pore aperture of 0.36 × 0.48 nm). More importantly, CO_2 possesses higher polarizability (26.3 × 10^{-25} cm^3) and quadrupole moment (13.4 × 10^{-40} C m^2), which results in stronger electronic interaction between CO_2 molecules and the inorganic framework.

IAST is one of the most credible theories to predict the multicomponent adsorption equilibrium with only the pure component adsorption isotherms. Herein, IAST was employed to predict CO_2/N_2 selectivity on the basis of the adsorption isotherms of CO_2 and N_2 at 273 and 298 K on SAPO-35_x samples (Fig. 2 and S6†) to investigate the influence of Si content and acidity on the CO_2 adsorption selectivities over N_2. The adsorption capacities are in the order CO_2 > N_2 for each sample, indicating the preferential adsorption for CO_2 over N_2. The Langmuir–Freundlich model fitted isotherm parameters were applied to carry out the calculations. The simulations were

Table 1 CO_2 adsorption and Q_{st} at zero coverage of SAPO-35_*x* at 273, 283 and 298 K

		CO_2 at 100 kPa (mmol g^{-1})			CO_2 at 10 kPa (mmol g^{-1})		
Sample	Q_{st} (kJ mol^{-1})	273 K	283 K	298 K	273 K	283 K	298 K
SAPO-35_0.08	26.0	3.80	3.21	2.53	1.37	1.00	0.71
SAPO-35_0.14	29.3	4.76	4.15	3.40	1.95	1.48	1.02
SAPO-35_0.22	27.5	3.87	3.41	2.69	1.40	1.06	0.71

conducted on gas mixtures with two different molar compositions (50/50 and 20/80 for CO_2/N_2). The adsorption isotherms were properly fitted by the dual-site Langmuir–Freundlich adsorption model (R^2 > 0.999, Fig. S7†). Subsequently, the fitting parameters (Tables S4–S6†) were applied in predicting the multicomponent adsorption with IAST. As shown in Fig. 3, the tendencies in the pressure dependence of IAST selectivity are similar among these three samples, *i.e.*, the selectivity falls rapidly at first and is later followed by a smaller dependence of selectivity on pressure. This is due to the heterogeneous adsorption site distribution on the zeolite cavities.

At lower pressures, the high-energy adsorption sites, *i.e.*, Brønsted acid sites in SAPO-based materials, are preferentially occupied by CO_2 molecules. As a result, the CO_2–adsorbent interaction is more pronounced than that at higher pressures.[12b,29] SAPO-35_0.14 shows the highest CO_2/N_2 IAST selectivity (49.9) at 298 K compared to the other two samples due to the increased acid strength and acidic concentration (Table 2). Compared to some other types of zeolites and adsorbing materials (Table S7†), SAPO-35_0.14 shows exhilarating separation selectivities for CO_2/N_2. In addition, Brønsted acid sites are highly polarized hydroxyl groups in zeolite frameworks.[12a] An increase of the concentration of acid sites generates more energetic adsorption sites for the quadrupolar adsorbate.[27c] Therefore, SAPO-35_0.14 is accompanied by the strongest electrostatic field. Consequently, the electronic interaction becomes stronger, which leads to the best CO_2 adsorption abilities. What's more, CO_2 is more polar than N_2, and the interaction between CO_2 molecules and the **LEV** framework shows higher sensitivity with the variation of the electrostatic field, thus SAPO-35_0.14 shows the highest CO_2/N_2 separation selectivity. To compare the separation performance of SAPO-35 made using NMP and HMI as templates, we synthesized SAPO-35 using HMI, named SAPO-35_HMI,[24a] which possesses the same Si content as the best adsorbent (SAPO-35_0.14). CO_2 and N_2 adsorption of SAPO-35_HMI and CO_2/N_2 IAST selectivity for SAPO-35_HMI at 273 K are shown in Fig. S8 and S9.† A comparison of CO_2 uptake and CO_2/N_2 IAST selectivity for SAPO-35_HMI and SAPO-35_0.14 is summarized in Table S8.† As a result, SAPO-35_HMI shows lower CO_2 uptake

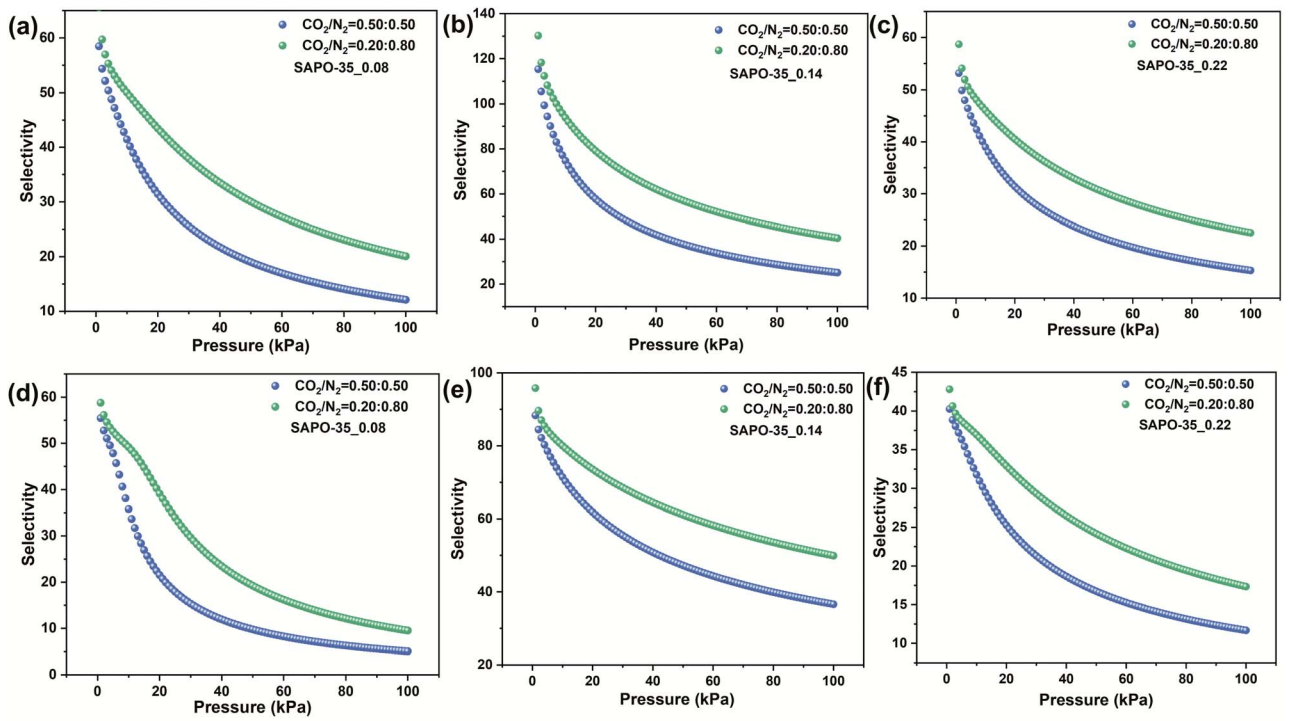

Fig. 3 CO_2/N_2 IAST selectivity for (a) SAPO-35_0.08, (b) SAPO-35_0.14, and (c) SAPO-35_0.22 at 273 K and (d) SAPO-35_0.08, (e) SAPO-35_0.14, and (f) SAPO-35_0.22 at 298 K.

Table 2 CO_2/N_2 IAST separation of SAPO-35_*x* at 273/298 K and 100 kPa

	CO_2/N_2 at 273 K		CO_2/N_2 at 298 K	
Sample	0.5 : 0.5	0.2 : 0.8	0.5 : 0.5	0.2 : 0.8
SAPO-35_0.08	12.1	20.1	5.1	9.5
SAPO-35_0.14	25.1	40.4	36.6	49.9
SAPO-35_0.22	15.3	22.5	11.7	17.3

and CO_2/N_2 selectivity compared with SAPO-35_0.14, proving the advantage of SAPO-35 zeolite synthesized using NMP as a template in CO_2 adsorption and separation application.

Breakthrough experiments

The breakthrough experiments of SAPO-35_0.14 were performed by utilizing binary CO_2/N_2 (20 : 80 v/v) gas mixtures at 298 K and atmospheric pressure in a fixed bed continuous separation system (Fig. S10†), imitating the industrial process conditions of flue gas.[1b,22] The corresponding breakthrough curves are displayed in Fig. 4. As shown in Fig. 4a, when the CO_2/N_2 mixture at a rate of 3.0 mL min^{-1} was fed into 5.80 g of SAPO-35_0.14 adsorbent, N_2 eluted first through the column without CO_2 breakthrough. However, the outlet concentration of CO_2 was below the detection limit of the FID until 800 seconds because CO_2 adsorbed on SAPO-35_0.14. When the pores of SAPO-35_0.14 progressively filled with CO_2, CO_2 began to break through the column and diluted the N_2. Hence, dynamic gas separation was achieved by selective CO_2 adsorption to SAPO-35_0.14. In line with equilibrium isotherms, the higher affinity of SAPO-35_0.14 for CO_2 over N_2 led to adequately long differences in breakthrough times. SAPO-35_0.14 is highly selective under dynamic conditions, hence we carried out multiple consecutive tests (Fig. 4b), and the results showed that the adsorption capacity of SAPO-35_0.14 fully recovered to its initial capacity, proving that SAPO-35_0.14 has excellent regeneration. In addition, for CO_2 capture from flue gas, it is important to evaluate the capacity and selectivity of adsorbents in the presence of water. We performed multiple consecutive breakthrough experiments of SAPO-35_0.14 with a relative humidity of ~40% by using a vapor generator at 298 K and 1 bar. The corresponding breakthrough curves are displayed in Fig. S11.† SAPO-35_0.14 well maintains its adsorption and separation abilities and regeneration in the presence of water, indicating the potential of the adsorbent for selective CO_2 adsorption in practical application.

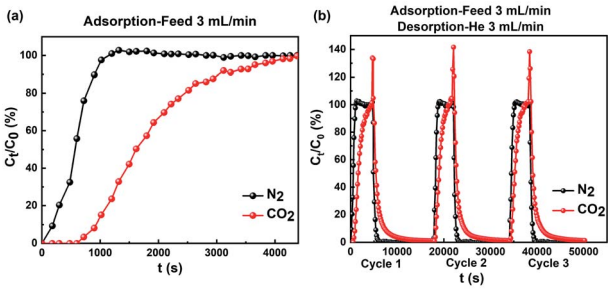

Fig. 4 (a) Experimental binary breakthrough curves for a gas mixture of CO_2/N_2 (20 : 80 v/v) on SAPO-35_0.14 at 298 K and 100 kPa with a total gas flow rate of 3 mL min^{-1}. C_t and C_0 denote outlet and inlet concentrations, respectively. (b) Multiple consecutive cycles of breakthrough curves for SAPO-35_0.14 with an adsorption/desorption gas flow rate of 3 mL min^{-1} (CO_2/N_2 20 : 80 v/v for adsorption and He for desorption) at 298 K and 100 kPa.

Conclusions

Zeolite materials are widely applied in CO_2 adsorption and separation. In particular, small-pore SAPO zeolites with 8-ring windows and high regenerability are potential candidates. In this work, we have first demonstrated that SAPO-35 zeolites with **LEV** topology possess excellent CO_2 adsorption and separation abilities. By using *N*-methylpiperidine (NMP) as a template, SAPO-35 zeolites with a broad range of Si contents were prepared, and their CO_2 adsorption/separation properties were investigated. Regulating the Si content can enhance the acidity and polarity of SAPO-35_0.14. Consequently, SAPO-35_0.14 showed a relatively higher CO_2 adsorption uptake of 4.76 mmol g^{-1} (273 K and 100 kPa) among aluminosilicate zeolites with the same topology (Na-LEV) and most of the SAPO zeolites, showing great potential for CO_2 adsorption. In the meantime, enhanced selectivities of CO_2/N_2 were also observed. Among these, SAPO-35_0.14 showed the highest CO_2/N_2 IAST selectivity of 49.9 at 298 K. SAPO-35_0.14 was also highly selective and was regenerated in transient breakthrough experiments, proving the potential of SAPO-35 zeolite in the practical selective CO_2 adsorption process. This work provides a powerful way to enhance the CO_2 adsorption properties of SAPO zeolites *via* regulating the Si content and acidity, which is of great significance for achieving superior CO_2 adsorption and separation abilities.

Author contributions

X. S. and J. Y. designed and supervised the project; Y. L. and C. W. performed the experiments; Y. Y. checked the data; H. C. and L. L. conducted the adsorption analyses; Y. L. wrote the first draft; X. S. and J. Y. deeply revised the manuscript.

Conflicts of interest

There are no conflicts to declare.

Acknowledgements

We thank the National Natural Science Foundation of China (grants 21920102005, 21835002, 21621001, 21871104, 21922810 and 22090062), the National Key Research and Development Program of China (Grant 2021YFA 1501202) and the 111 Project (B17020) for supporting this work.

References

1 (*a*) D. M. D'Alessandro, B. Smit and J. R. Long, *Angew. Chem., Int. Ed.*, 2010, **49**, 6058–6082; (*b*) Y.-S. Bae and R. Q. Snurr, *Angew. Chem., Int. Ed.*, 2011, **50**, 11586–11596.

2 H. A. Patel, J. Byun and C. T. Yavuz, *ChemSusChem*, 2017, **10**, 1303–1317.
3 R. Liu, S. Xu, G. Hao and A. Lu, *Chem. J. Chinese Universities*, 2022, **38**, 18–30.
4 (*a*) M. R. Hudson, W. L. Queen, J. A. Mason, D. W. Fickel, R. F. Lobo and C. M. Brown, *J. Am. Chem. Soc.*, 2012, **134**, 1970–1973; (*b*) S. Smeets, D. Xie, L. B. McCusker, C. Baerlocher, S. I. Zones, J. A. Thompson, H. S. Lacheen and H.-M. Huang, *Chem. Mater.*, 2014, **26**, 3909–3913; (*c*) Y. Chai, X. Han, W. Li, S. Liu, S. Yao, C. Wang, W. Shi, I. da-Silva, P. Manuel, Y. Cheng, L. D. Daemen, A. J. Ramirez-Cuesta, C. C. Tang, L. Jiang, S. Yang, N. Guan and L. Li, *Science*, 2020, **368**, 1002–1006.
5 (*a*) H.-M. Wen, B. Li, L. Li, R.-B. Lin, W. Zhou, G. Qian and B. Chen, *Adv. Mater.*, 2018, **30**, 1704792; (*b*) H. Zeng, M. Xie, T. Wang, R.-J. Wei, X.-J. Xie, Y. Zhao, W. Lu and D. Li, *Nature*, 2021, **595**, 542–548.
6 A. G. Kontos, V. Likodimos, C. M. Veziri, E. Kouvelos, N. Moustakas, G. N. Karanikolos, G. E. Romanos and P. Falaras, *ChemSusChem*, 2014, **7**, 1696–1702.
7 O. F. Altundal, C. Altintas and S. Keskin, *J. Mater. Chem. A*, 2020, **8**, 14609–14623.
8 Y. Liu, S. Wang, X. Meng, Y. Ye, X. Song, Z. Liang and Y. Zhao, *Angew. Chem., Int. Ed.*, 2020, **59**, 19487–19493.
9 G. Férey, *Chem. Soc. Rev.*, 2008, **37**, 191–214.
10 (*a*) Y. Li and J. Yu, *Nat. Rev. Mater.*, 2021, **6**, 1156–1174; (*b*) Q. Sun, Z. Xie and J. Yu, *Natl. Sci. Rev.*, 2017, **5**, 542–558; (*c*) Z. Wang, J. Yu and R. Xu, *Chem. Soc. Rev.*, 2012, **41**, 1729–1741; (*d*) L. Yu, X. Shang, H. Chen, L. Xiao, Y. Zhu and J. Fan, *Nat. Commun.*, 2019, **10**, 1932; (*e*) D.-D. Zhou, X.-W. Zhang, Z.-W. Mo, Y.-Z. Xu, X.-Y. Tian, Y. Li, X.-M. Chen and J.-P. Zhang, *EnergyChem*, 2019, **1**, 100016.
11 (*a*) J. Shang, G. Li, R. Singh, Q. Gu, K. M. Nairn, T. J. Bastow, N. Medhekar, C. M. Doherty, A. J. Hill, J. Z. Liu and P. A. Webley, *J. Am. Chem. Soc.*, 2012, **134**, 19246–19253; (*b*) P. Li and F. Handan Tezel, *Microporous Mesoporous Mater.*, 2007, **98**, 94–101.
12 (*a*) Y. Li, L. Li and J. Yu, *Chem*, 2017, **3**, 928–949; (*b*) Y. Guo, T. Sun, Y. Gu, X. Liu, Q. Ke, X. Wei and S. Wang, *Chem. Asian J.*, 2018, **13**, 3222–3230; (*c*) M. Pera-Titus, *Chem. Rev.*, 2014, **114**, 1413–1492.
13 Q. Yue, J. Halamek, D. N. Rainer, J. Zhang, R. Bulánek, R. E. Morris, J. Čejka and M. Opanasenko, *Chem. Eng. J.*, 2022, **429**, 131277.
14 M. Moliner, C. Martínez and A. Corma, *Chem. Mater.*, 2014, **26**, 246–258.
15 J. Yang, J. Li, W. Wang, L. Li and J. Li, *Ind. Eng. Chem. Res.*, 2013, **52**, 17856–17864.
16 A. Zukal, M. Shamzhy, M. Kubů and J. Čejka, *J. CO_2 Util.*, 2018, **24**, 157–163.
17 (*a*) J. Gong, C. Wang, C. Zeng and L. Zhang, *Microporous Mesoporous Mater.*, 2016, **221**, 128–136; (*b*) Y. Wang, Q. Zhang and J. Yu, *Chem. J. Chin. Univ.*, 2020, **41**, 616–622.
18 M. M. Lozinska, E. Mangano, J. P. S. Mowat, A. M. Shepherd, R. F. Howe, S. P. Thompson, J. E. Parker, S. Brandani and P. A. Wright, *J. Am. Chem. Soc.*, 2012, **134**, 17628–17642.
19 Y. Yu, X. Li, R. Krishna, Y. Liu, Y. Cui, J. Du, Z. Liang, X. Song and J. Yu, *ACS Appl. Mater. Interfaces*, 2018, **10**, 43570–43577.
20 H. J. Choi and S. B. Hong, *Chem. Eng. J.*, 2022, **433**, 133800.
21 T. D. Pham, M. R. Hudson, C. M. Brown and R. F. Lobo, *ChemSusChem*, 2017, **10**, 946–957.
22 X. Wang, N. Yan, M. Xie, P. Liu, P. Bai, H. Su, B. Wang, Y. Wang, L. Li, T. Cheng, P. Guo, W. Yan and J. Yu, *Chem. Sci.*, 2021, **12**, 8803–8810.
23 (*a*) O. Cheung and N. Hedin, *RSC Adv.*, 2014, **4**, 14480–14494; (*b*) M. Palomino, A. Corma, J. L. Jordá, F. Rey and S. Valencia, *Chem. Commun.*, 2012, **48**, 215–217; (*c*) R. L. Siegelman, E. J. Kim and J. R. Long, *Nat. Mater.*, 2021, **20**, 1060–1072.
24 (*a*) O. Cheung, Q. Liu, Z. Bacsik and N. Hedin, *Microporous Mesoporous Mater.*, 2012, **156**, 90–96; (*b*) B. M. Lok, C. A. Messina, R. L. Patton, R. T. Gajek, T. R. Cannan and E. M. Flanigen, *J. Am. Chem. Soc.*, 1984, **106**, 6092–6093.
25 H. J. Jung, C. H. Shin and S. B. Hong, *J. Phys. Chem. B*, 2005, **109**, 20847–20853.
26 (*a*) I. Pinilla-Herrero, U. Olsbye, C. Márquez-Álvarez and E. Sastre, *J. Catal.*, 2017, **352**, 191–207; (*b*) I. Pinilla-Herrero, C. Marquez-Alvarez and E. Sastre, *Catal. Sci. Technol.*, 2017, **7**, 3892–3901.
27 (*a*) L. S. de Saldarriaga, C. Saldarriaga and M. E. Davis, *J. Am. Chem. Soc.*, 1987, **109**, 2686–2691; (*b*) D. Barthomeuf, *Zeolites*, 1994, **14**, 394–401; (*c*) I. Deroche, L. Gaberova, G. Maurin, M. Castro, P. A. Wright and P. L. Llewellyn, *J. Phys. Chem. C*, 2008, **112**, 5048–5056.
28 J. Yang, Q. Zhao, H. Xu, L. Li, J. Dong and J. Li, *J. Chem. Eng. Data*, 2012, **57**, 3701–3709.
29 X. Su, P. Tian, D. Fan, Q. Xia, Y. Yang, S. Xu, L. Zhang, Y. Zhang, D. Wang and Z. Liu, *ChemSusChem*, 2013, **6**, 911–918.